On normal and anomalous self-diffusion in body-centred cubic metals: a computer simulation study

1993 J. Phys.: Condens. Matter 5 9121

(http://iopscience.iop.org/0953-8984/5/49/014)

J. Phys.: Condens. Matter 5 (1993) 9121–9130. Printed in the UK

On normal and anomalous self-diffusion in body-centred cubic metals: a computer simulation study

A G Mikhin and Yu N Osetsky†

Russian Scientific Centre 'Kurchatov Institute', Kurchatov Square 1, 123182 Moscow, Russia

Received 26 February 1993, in final form 1 September 1993

Abstract. A computer simulation study of the lattice dynamics and vacancy migration of BCC Fe and in BCC Zr is presented. The results obtained are in good agreement with experiments. Special attention is paid to the temperature behaviour of the $T_1\frac{1}{2}(110)$ phonon mode. This mode in Zr is shown to be related to the β-to-α phase transformation as well as to the curvature of the Arrhenius plot. A phonon-enhanced mechanism with a temperature-dependent vacancy migration enthalpy is proposed as an explanation of 'anomalous' self-diffusion in BCC metals.

1. Introduction

BCC metals are conventionally classified in two groups with regard to self-diffusion:

(i) 'normal' metals such as Cr, Mo, W and Fe, which exhibit linear dependences of the diffusion coefficient versus normalized temperature T_m/T (where T_m is the melting temperature) with the parameters obeying the well known semi-empirical relations;

(ii) 'anomalous' metals such as β-Ti, β-Zr and β-Hf, in which the diffusivities are much faster than those in (i) and the Arrhenius plots are strongly curved (see e.g., [1]).

Various hypotheses have been advanced in order to explain these anomalies. The recent most promising models confirm the monovacancy mechanism [2] and suggest that the diffusion processes in (ii) are dominantly controlled by certain soft and temperature-dependent phonon modes. Thus, Herzig and Kohler [1] examine the $L\frac{2}{3}(111)$ mode, while Petry *et al* [3] consider the $T_1\frac{1}{2}(110)$ mode. It is important that these two types of Brillouin zone boundary phonon are related to the displacements necessary for high-pressure BCC-to-ω and low-temperature BCC-to-HCP phase transformations, respectively. Furthermore, the extensive phonon measurements by Petry *et al* (see, e.g., [4]) have revealed that both types of phonon are overdamped and have a very low energy but only a $T_1\frac{1}{2}(110)$ mode (hereafter denoted the T_1 N-point phonon mode) is temperature dependent.

Attempts have been made to clarify diffusion phenomena in (ii) by computer simulations. For instance, Willaime and Massobrio [5–7] have developed a model for Zr based on the N-body interatomic potential which reproduces some properties of HCP and BCC Zr. In particular, the low frequencies of the $L\frac{3}{2}(111)$ and $T_1\frac{1}{2}(110)$ phonon modes [6] as well as an essentially low vacancy migration energy $H_v^m = 0.28$ eV [7] have been obtained. Nevertheless, neither a strong temperature dependence of the above phonons nor a curvature

† Present address: Departament de Matematica Aplicada III, Universitat Politecnica de Catalunya, ETSE Camins, Gran Capitan, s/n, Edifici C2, 08034 Barcelona, Spain.

0953-8984/93/499121+10$07.50

of the Arrhenius plot has been displayed. In our preliminary work on vacancy migration in BCC Zr [8] we have found two pronounced regions in the plot of the vacancy jump rate versus the reciprocal temperature with $H_v^m = 0.33$ eV (2000 K $> T >$ 1500 K) and $H_v^m = 0.12$ eV (1400 K $> T >$ 1100 K). However, the phonon properties, phase transformations and vacancy migration mechanism were not investigated sufficiently well in that work.

In this paper we present in brief the results of computer simulations of the lattice dynamics via the quasi-harmonic approximation (QHA) and molecular dynamics (MD), of the BCC-to-HCP and BCC-to-ω phase transformations, and of the vacancy migration mechanism in 'normal' BCC Fe and 'anomalous' BCC Zr.

2. Potentials and calculation model

All calculations are performed within the transition-metal model [9] based on the generalized pseudopotential theory [10, 11]. As was shown by Moriarty, [10, 11] the transition-metal pair potential may be written as

$$V_{tot}(r) = V_{sc}(r) + V_d(r) + V_{ol}(r). \tag{1}$$

The first term represents the screened Coulomb interaction which, in the second-order approximation, has the form [12]

$$V_{sc}(r) = \frac{Z^2}{r} - \frac{1}{8\pi^3 r}\int_0^\infty q^3 v^2(q)\left(1 - \frac{1}{\epsilon(q)}\right)\sin(qr)\,dq \tag{2}$$

where Z is the effective valence, $\epsilon(q)$ is the dielectric function in the Geldart–Taylor approximation [13] and $V(q)$ is the Fourier transform of the local pseudopotential. Here we use the model pseudopotential of Animalu and Heine [13]:

$$V(q) = -(4\pi Z/q^2)\{\cos(qR_s) + U_s[[\sin(qR_s)/qR_s] - \cos(qR_s)]\}\exp(-\gamma q^4/16k_F^4) \tag{3}$$

where k_F is the Fermi momentum, and R_s, U_s and γ are parameters. The applicability of this pseudopotential to transition metals was discussed in [12].

The second term in (1) describes the volume-dependent d-electron interactions. According to Moriarty [10], the pair part of these interactions may be written in the form

$$V_d(r) = C_2(r_0/r)^{20} - C_1(r_0/r)^{10} \tag{4}$$

where $r_0 = 1.8R_{WS}$ (R_{WS} is the Wigner–Seitz radius), and C_1 and C_2 are material-related parameters which depend on d-band filling and width.

The third term in (1) represents the short-range overlap potential. Here we use the simple Born–Mayer potential

$$V_{ol}(r) = A\exp(-Br) \tag{5}$$

with A and B as parameters.

The detailed description of the fitting procedure and testing of this type of potential for different metals will be presented in [14]. Here we note only that the pseudopotential parameters R_s, U_s and γ as well as the parameters A and B were determined by fitting

to the equilibrium lattice parameter, bulk modulus and some points of phonon dispersion curves of HCP Zr and BCC Fe. The parameters C_1 and C_2 were specified in accordance with the filling and width of the d zone [15, 16], and the effective valence Z was assumed to be near first-principle valences [17]. It should be noted that the potential for HCP Zr was used successfully in [18] to study the features of the anisotropy of the migration of vacancies and interstitials.

The parameters obtained for HCP Zr were then used to construct a potential for BCC Zr. The elastic constants, the enthalpy difference between the BCC and HCP phases and the monovacancy properties calculated by statical simulation of BCC Zr and BCC Fe are listed in table 1. It can be seen that the agreement between the calculated and experimental quantities is quite good not only for Fe but also for BCC Zr.

Table 1. Physical quantities for BCC Fe and BCC Zr calculated with the QHA at 0 K and zero pressure and compared with the experimental values for α-Fe and β-Zr from [12] (room temperature) and [4] ($T = 915$ K), respectively. a is the lattice parameter, $\Delta H = H_{BCC} - H_{HCP}$ is the enthalpy difference between BCC and HCP phases, B, C_{44} and C' are the elastic moduli, and H_v^f and H_v^m are the vacancy formation and migration enthalpies, respectively.

	a (Å)	ΔH (eV/atom)	B (GPa)	C_{44} (GPa)	C' (GPa)	H_v^f (eV)	H_v^m (eV)
Fe, calculated	2.87	−0.07	181	114	50	1.94	0.78
Fe, experimental	2.87	—	168	118	49	≃2.00	≃0.6–1.3
Zr, calculated	3.58	0.03	86	67	0.4	1.15	0.51
Zr, experimental	3.57[a]	0.04	97	38	5.5	—	—

[a] Extrapolation at 0 K of the linear fit to the experimental values from [4].

Using this potential and different MD techniques we studied phonon properties, phase transformations and vacancy migration. To study the vacancy migration mechanisms we used the usual MD technique for a crystal of 1457 movable atoms oriented along [100], [010] and [001] axes with periodic boundary conditions. During our calculation the time step was $t_0 = 1 \times 10^{-15}$ s. We used three series of simulations with different initial velocity distributions for each temperature. Each series collected about 50–100 vacancy jumps which required about 100 000–200 000 time steps depending on the temperature. A study of the temperature behaviour of phonon modes was carried out for the same crystals using the perturbation technique [19]. The simulation of phase transformations was performed at a constant temperature and constant pressure by employing the Parinello–Rahman and Nose techiques [20]. For these simulations we used crystals containing 264–800 movable atoms oriented along [100], [011] and [0$\bar{1}$1] directions. Note that during all the calculations we took into account the change in atomic volumes for both metals due to the thermal lattice expansion.

3. Results and discussion

It was supposed that the temperature behaviour of phonons is the key to understanding the anomalous diffusion phenomenon; so we paid special attention to the features of the phonon behaviour in BCC Fe and BCC Zr.

The phonon dispersion curves calculated for zero temperature in the BCC phases of Fe and Zr via the QHA are presented in figure 1. It is easy to see that the curves obtained for

both metals compare well with the experimental points from [4,21]. Moreover, for BCC Zr, our model reproduces the extremely low-lying T_1 [110] branch. In particular, the shear modulus $C' = \frac{1}{2}(C_{11} - C_{12})$ (see table 1) is close to zero. These facts show the mechanical instability of the BCC lattice in the QHA with respect to the BCC-to-HCP transformation as predicted by the *ab-initio* frozen-phonon calculations [22]. It should be noted that the Zr model in [6] also describes such features of phonons in BCC Zr within the QHA. A study of phonon temperature behaviour within the QHA shows us a weak frequency decrease for all symmetry point phonons.

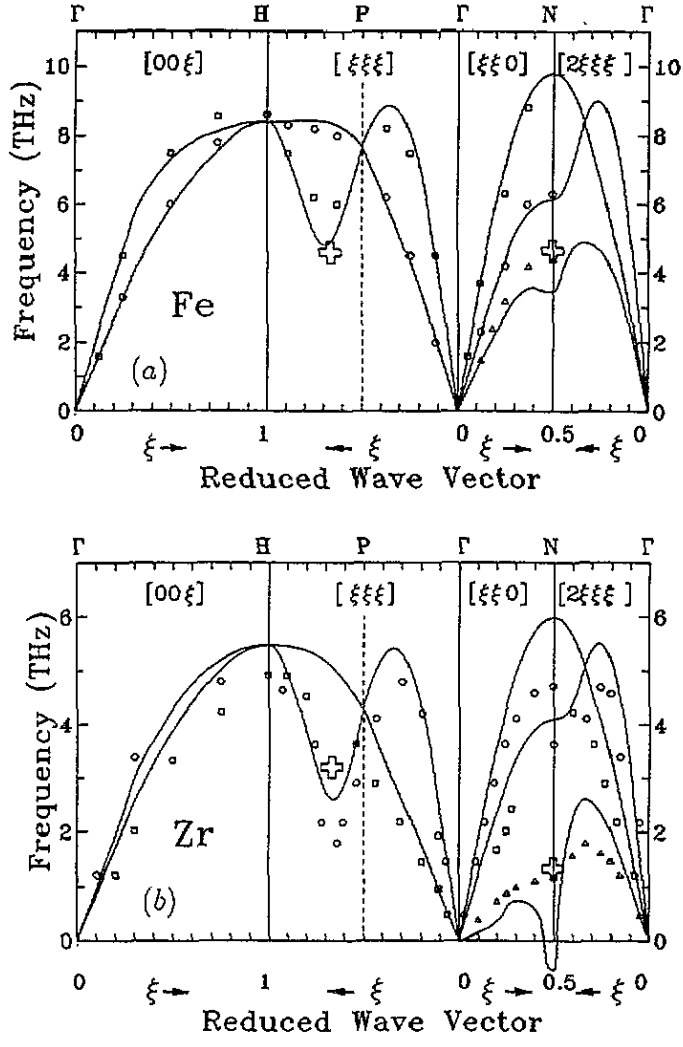

Figure 1. Phonon dispersion curves of (*a*) BCC Fe at 295 K and (*b*) BCC Zr at 1188 K; ——, results of the QHA calculations; ○, □, experimental results from [12] and [4], respectively; the crosses are results of the MD computations at 1200 K.

Qualitatively another result was obtained when we studied the temperature behaviour of the $L\frac{2}{3}(111)$ mode and the $T_1\frac{1}{2}(110)$ mode with $[\bar{1}10]$ polarization by applying the MD

and the perturbation techqniques. It was found that the frequencies of both modes for BCC Fe and the former mode for BCC Zr decrease weakly as the temperature increases as well as in the QHA. However, contrary to the quasi-harmonic calculations, the MD data demonstrate the small but real frequency of the T_1 N-point phonons in BCC Zr (see figure 1(*b*)) which increases significantly with increasing temperature (see figure 2). This phonon temperature behaviour compared remarkably well with the experimental results [4]. Note that the results on phonon temperature behaviour obtained in [6] demonstrated a very weak temperature dependence (open squares in figure 2).

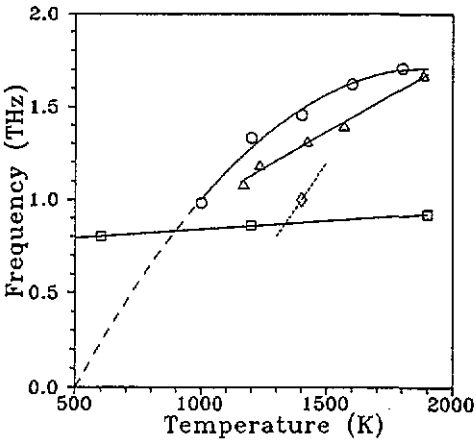

Figure 2. Temperature dependences of the frequencies of the T_1 N-point phonons: ○, MD computation; – – –, extrapolation of MD computation to the low-temperature region; △, experimental values [4]; □, MD computations [6]; ◇, *ab-initio* calculations [22]; · · · · · ·, predicted dependence of *ab-initio* calculations.

Thus, our computations confirm the importance of the excess vibrational entropy due to the low-energy $T_1[110]$ branch in stabilizing the BCC structure of Zr at high temperatures [4]. The temperature dependences of other phonons at the symmetric points in BCC Zr and all phonons in BCC Fe are quite weak and they are well described by the QHA.

These results are in good correlation with simulations of the phase transformation. As expected from the phonon properties, BCC Fe is found to be stable with regard to the BCC-to-HCP transformation over the whole temperature range investigated (1000 K $< T <$ 2000 K), while BCC Zr transforms into the HCP structure at $T < T_{\beta\to\alpha} = 1250$ K (experimental temperature $T^{\exp}_{\beta\to\alpha} = 1135$ K) according to the Burgers mechanism as in [5]. As for the BCC-to-ω phase transformation, the stable ω structure was not found for both metals over the whole temperature range and pressure range (0–250 kbar) used.

Finally, we carried out a vacancy migration study by MD at constant pressure. In both metals the vacancy is observed to migrate mostly via nearest-neighbour jumps. Only a few fast vacancy jumps into third- and fifth-neighbour sites were found for high pre-melting temperatures. However, these very scarce events do not affect the total vacancy jump rate. The temperature dependences of the vacancy jump rate $\Gamma(T)$ for BCC Zr and BCC Fe are presented in figure 3. Note how the behaviour for BCC Fe is linear whereas it is not linear for BCC Zr, in qualitative agreement with tracer diffusion measurements [1]. Therefore, $\Gamma(T)$ for BCC Fe can be expressed in terms of the Arrhenius relation

$$\Gamma(t) - \Gamma_0 \exp(-G^{\mathrm{m}}_{\mathrm{v}}/kT) = \Gamma'_0 \exp(-H^{\mathrm{m}}_{\mathrm{v}}/kT) \tag{6}$$

with

$$G_v^m = H_v^m - TS_v^m. \tag{7}$$

Here G_v^m, H_v^m and S_v^m are the free energy, the enthalpy and the entropy, respectively, of the vacancy migration, and Γ_0 is the attempt frequency. For BCC Fe the best fit of equation (6) to the results obtained gives $\Gamma_0' = 2.2 \times 10^{14}$ s^{-1} and $H_v^m = 0.85$ eV. Note that the vacancy migration enthalpy derived from MD is slightly larger than from static calculations (see table 1). The same treatment for BCC Zr gives the values $\Gamma_0' = 1.5 \times 10^{13}$ s^{-1} and $H_v^m = 0.38$ eV but describes the results obtained quite unsatisfactorily.

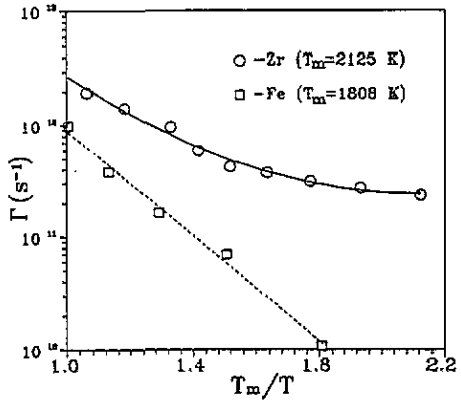

Figure 3. Vacancy jump rate versus normalized reciprocal temperature for BCC Fe and BCC Zr.

Taking into account the above phonon considerations we associate unambiguously the curvature of $\Gamma(T)$ for BCC Zr with the T_1 N-point phonon softening as the temperature decreases to $T_{\beta\to\alpha}$. So, it is reasonable to assume that equation (7) is too simple to describe G_v^m for BCC Zr, which follows a more complex temperature dependence. We suggest that there are two kinds of phonon mode which are responsible for vacancy migration. We call the first type the 'normal modes'; these are described by QHA qualitatively and their frequencies decrease weakly as the temperature increases. We call the second strongly anharmonic type the 'anomalous modes' and their frequencies increase with increasing temperature. The latter are mainly the $T_1\frac{1}{2}(110)$ phonons. To describe the curvature of the Arrhenius plot for BCC Zr we substitute for the following expression for the free energy of vacancy migration for equation (7):

$$G_v^m(T) = G_0^m + G_1^m T + G_{-1}^m/T \tag{8}$$

where the term $G_1^m T$ is connected with the normal quasi-harmonic modes and the term G_{-1}^m/T with the anomalous modes. Comparing these with the thermodynamic parameters, we can attribute G_0^m to H_v^m and G_1^m to $-S_v^m$. Then, following [23], we introduce the anomaly parameter for vacancy migration: $A^m = -G_{-1}^m$. Combination of equation (8) with equation (6) gives

$$\Gamma(T) = \Gamma_0' \exp(-H_v^m/kT) \exp(A^m/kT^2). \tag{9}$$

For BCC Zr the best three parameters that fit equation (9) to the results obtained are $\Gamma_0' = 1.7 \times 10^{15}$ s^{-1}, $H_v^m = 1.5$ eV and $A^m = 760$ eV K. As shown in figure 3 (full

curve), equation (9) with the above parameters allows us to describe $\Gamma(T)$ for BCC Zr quite well. Let us try to find the physical meaning of the above parameters. As follows from equation (9), H_v^m is the vacancy migration enthalpy for very high temperatures when the second exponent in (9) is close to unity. In addition, for these temperatures we shall have quite a straight Arrhenius plot. However, these temperatures lie out of the range of existence of BCC Zr. Therefore, for realistic temperatures, we have a curved Arrhenius plot and an effective vacancy migration enthalpy (which may be determined as the slope of Arrhenius plot for particular temperatures) less than H_v^m. Moreover, we can find the temperature T_0 when the effective vacancy migration enthalpy is equal to zero:

$$H_v^m - A^m/T_0 = 0. \tag{10}$$

For the above parameters the temperature $T_0 = 500$ K, and therefore it lies much lower than the BCC-to-HCP phase transition temperature $T_{\beta\to\alpha} = 1250$ K. Thus, H_v^m is the vacancy migration enthalpy for the hypothetical high-temperature 'non-anomalous' BCC Zr and A^m is related to the temperature of the 'low-temperature instability' of BCC Zr. It is clear that this 'low-temperature instability' obtained from vacancy migration must reflect the instability of phonons which are responsible for this anomaly. So, it is not surprising that T_0 coincides with the extrapolated temperature of zero frequency of the T_1 N-point phonons (see figure 2). We think that this coincidence confirms the important role of the $T_1\frac{1}{2}(110)$ phonons in the vacancy migration anomaly in BCC Zr.

In relation to BCC Fe, the treatment of $\Gamma(T)$ by equation (9) leads to $\Gamma_0' = 2.3\times10^{14}$ s^{-1}, $H_v^m = 0.86$ eV and $A^m = 3$ eV K. Thus, in the case where there is no anomaly in the phonon behaviour, we obtained a very small anomaly parameter for vacancy migration in BCC Fe and exactly the same values of attempt frequency and vacancy migration enthalpy as using equation (6).

Therefore, the results obtained by MD simulation of vacancy migration show that the migration enthalpy for BCC Fe is constant while the effective vacancy migration enthalpy for BCC Zr is strongly temperature dependent.

From static calculations for BCC Fe we obtained $H_v^m = 0.78$ eV. It is clear that the static technique allows us to estimate the lower limit of this value as in an adiabatic approximation. Indeed, the MD results for Fe gave us the alue $H_v^m = 0.85$ eV. Qualitatively this result is quite understandable for a system with only normal phonons. A similar result was obtained in [24] using a simpler long-range pair potential for BCC Fe. It is difficult to compare these results with experimental data because there is an uncertainty in the experimental results of 0.55–1.30 eV [25–28]. In [29] a relatively low enthalpy of 0.66 eV was also obtained. Nevertheless, we think that the larger value is more appropriate for a 'normal' metal, and therefore for α-Fe. Moreover, the vacancy migration enthalpy of about 0.9 eV is more consistent with the activation enthalpy for self-diffusion in α-Fe [30,31].

For BCC Zr we have quite another situation and the effective vacancy migration enthalpy varies from 0.24 eV (for $T = 1188$ K) to 0.79 eV (for $T = 2100$ K) in comparison with the static result $H_v^m = 0.51$ eV. This may be understood if we take into account the results obained for the temperature behaviour of anomalous phonons. At low temperatures near the phase transformation these phonons have low frequencies and are strongly temperature dependent. In our opinion this is why there is both fast vacancy migration by the mechanism discussed below and curvature of the Arrhenius plot. At high pre-melting temperatures the frequency of the T_1 N-point phonons is increased and the temperature dependence is weak. So the effect of these phonons on vacancy migration is decreased and we have a 'normal' vacancy migration similar to that for Fe. It is interesting also to note that our

vacancy migration enthalpy for BCC Zr at $T = 1188$ K is close to 0.28 eV, the value calculated for the same temperature in [29] by the treatment of phonon spectra of BCC Zr with the phonon-controlled vacancy migration model. However, we obtained larger vacancy migration enthalpy at a high temperature ($T = 1883$ K) than that in [29]: 0.71 eV instead of 0.37 eV. It seems to us that one possible reason for this may be the high frequency of $L\frac{2}{3}(111)$ phonons in our model of BCC Zr. A comparative analysis of the present results and those in [7, 8] allowed us to propose that these phonons determine the slope rather than the curvature of the Arrhenius plot. For example, the frequency and behaviour of these phonons in both BCC Fe and BCC Zr are similar in our model. At the same time in the high-temperature region, where the effect of the T_1 N-point phonons is weak, we obtained similar slopes of the Arrhenius plots (and therefore similar vacancy migration enthalpies) for the two metals. In view of this, the correlation between the activation energy for self-diffusion and the degree of the $L\frac{2}{3}(111)$ phonon softening in BCC metals reported by Herzig and Kohler [1] can be better understood.

Thus, we have more or less direct evidence of a close relationship between the frequency and temperature dependences of the T_1 N-point phonons and vacancy migration enthalpy.

Looking for the difference between the migration mechanisms in BCC Fe and BCC Zr, we investigated the temporary evolution of atomic displacements around a vacancy during the migration process. In the general case, the trajectory of the migrating atom is complex and deviates from the straight $\langle 111 \rangle$ path. However, careful analysis reveals the following features.

(1) The deviations in Zr are greater than those in Fe.

(2) The deviations in BCC Zr increase when approaching the BCC-to-HCP phase trnasformation.

Typical displacements in BCC Zr at low temperatures are shown in figure 4(a). The trajectory of the migrating atom with the elementary jump vector $\frac{1}{2}[\bar{1}\bar{1}1]$ can be approximately expanded in the (101) plane into three parts. The first and third parts coincide with the $[\bar{1}\bar{2}1]$ direction while the second is in the $[\bar{1}01]$ direction. Generalizing this expansion over all directions of vacancy jumps gives

$$\tfrac{1}{2}\langle 111 \rangle = \tfrac{1}{4}\langle 1, 1, 1 + \delta \rangle + \tfrac{1}{4}\langle 1, 1, 1 - \delta \rangle \tag{11}$$

where δ is the degree of deviation from the straight $\langle 111 \rangle$ path ($0 < \delta < 1$). For instance, for BCC Fe, δ is close to zero while, for BCC Zr, at low temperatures δ is about unity.

Further analysis for BCC Zr gives a migration mechanism enhanced by soft T_1 N-point phonons which can be outlined as follows. When the migrating atom moves into a vacant site, it goes through two triangular configurations formed by atoms in adjacent (111) planes, as illustrated in figure 4(b). The superposition of the T_1 N-point phonons promotes large $(11\bar{1})\langle 112 \rangle$ displacements in these triangles. These displacements are strongly spatially and temporally correlated so that the whole system acts as a 'double door'; that is, whereas the first triangle door is opening, the second is closing, and vice versa. Consequently the migrating atom should deviate from the straight $[\bar{1}\bar{1}1]$ path in order to find the most widely opened space. From an energy point of view this process implies an asymmetric double barrier for the migrating atom which changes periodically with a frequency close that of the T_1 N-point phonons. Note that a similar scenario has been discussed by Petry *et al* [3]. However, this situation is characteristic only for low temperatures. As the temperature rises, the frequencies of the T_1 N-point phonons rise also and conditions for a correlated 'double door' are disturbed. This leads to a more irregular but straighter path ($\delta \to 0$)

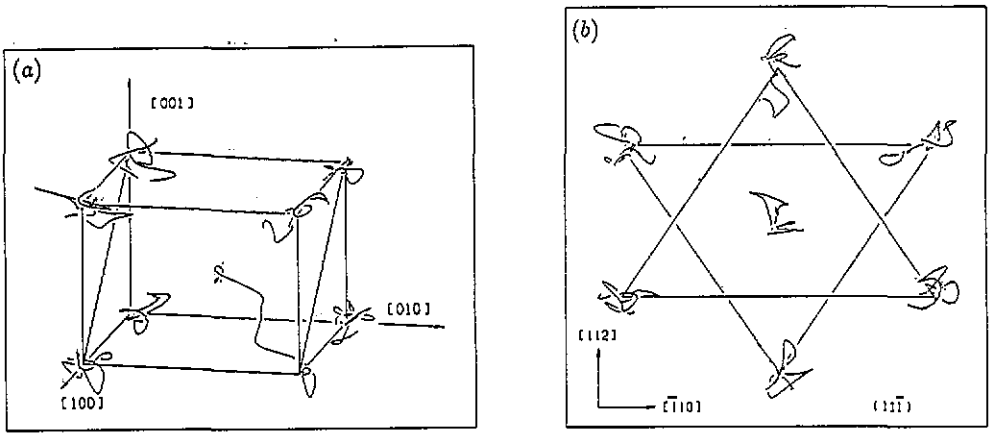

Figure 4. Atomic displacements around a vacancy during the migration process in BCC Zr at 1200 K: (*a*) nearest-neighbour atoms; (*b*) the (11$\bar{1}$) projection of the trajectory of the migrating atom (in the centre) and two triangular configurations.

for the migrating atom and to an increase in the effective vacancy migration energy. Thus, vacancy migration mechanisms for BCC Fe in the whole temperature range and for BCC Zr in the high-temperature range are very similar.

In principle, the existence of a dynamic asymmetric double barrier for vacancy migration was suggested earlier [32]. In this work the vacancy migration in BCC Fe was studied using MD and a short-range empirical potential. It was found that the vacancy jump rate is described very well by equation (6) and the dynamic vancancy migration energy (0.48 eV) was less than that from static calculation (0.60 eV). In [32] a dynamic double barrier was assumed to exist in order to explain this decrease in the migration energy. Qualitatively the same result—a straight Arrhenius plot and a dynamic vacancy migration energy less than the static value—was obtained in [7] for BCC Zr. We do not know the phonon properties for the potential used in [32] but we know that the potential used in [7] gives a very weak temperature dependence of the T_1 N-point phonons. When our results are taken into account, it is reasonable to suppose that both Willaime and Massobrio [7] and Tsai *et al* [32] observed the 'anomalous migration' of vacancies in BCC Fe and BCC Zr in the whole temperature range investigated and that they did not obtain the curvature of Arrhenius plots because the potentials used in [7, 32] do not describe the strong temperature dependence of the above phonons.

4. *Summary*

In summary, our model reproduces well the main properties of 'normal' BCC Fe and 'anomalous' BCC Zr. Within the framework of this model we found the phonon-enhanced mechanism of vacancy migration. According to this mechanism the self-diffusion anomalies for the BCC phases of the group IVb metals are induced by the particular behaviour of the $L\frac{2}{3}(111)$ and $T_1\frac{1}{2}(110)$ phonons or more generally of the $T_1\frac{1}{2}[112]$ branch. We demonstrated that the temperature-dependent $T_1\frac{1}{2}[110]$ mode provides the observed curvature of the Arrhenius plot while the $L\frac{2}{3}(111)$ mode seems to be responsible for the high level of

vacancy mobility. A more detailed picture of phonon-enhanced vacancy migration will be given elsewhere.

Acknowledgments

We wish to thank Professor V G Vaks and Dr A V Trefilov for their help in developing the interatomic potentials and Dr E A Smirnov and Professor M I Katsnelson for many constructive suggestions. We would also like to express our gratitude to Dr W Petry and Professor G Martin for fruitful discussions and supplying us with some valuable materials.

This work was partly supported by the Soros Foundation Grant awarded by the American Physical Society.

References

[1] Herzig C and Kohler U 1987 *Mater. Sci. Forum* **15–18** 301
[2] Vogl G, Petry W, Flottman Th and Heiming A 1989 *Phys. Rev.* B **39** 5025
[3] Petry W, Heiming A, Trampenau J and Vogl G 1988 *Proc. Int. Conf. on Diffusion in Metals and Alloys* (Aedermannsdorf: Trans Tech) p 157
[4] Heiming A, Petry W, Trampenau J, Alba M, Herzig C, Shober H R and Vogl G 1991 *Phys. Rev.* B **43** 10 948
[5] Willaime Fr and Massobrio C 1989 *Phys. Rev. Lett.* **63** 2244
[6] Willaime Fr and Massobrio C 1991 *Phys. Rev.* B **43** 11 653
[7] Willaime Fr and Massobrio C 1990 *Atomic Scale Calculation of Structures in Materials* ed M A Schlutter and M S Daw (Pittsburgh, PA: Materials Research Society) p 295
[8] Mikhin A G, Osetsky Yu N and Smirnov E A 1992 *Moscow Engineering Physics Institute, Russia, Annual Report* p 105
[9] Katsnelson M I, Mikhin A G, Osetsky Yu N and Trefilov A V 1992 unpublished
[10] Moriarty J A 1990 *Phys. Rev.* B **42** 1609
[11] Moriarty J A 1988 *Phys. Rev.* B **38** 3199
[12] Vaks V G, Kapinos V G, Osetsky Yu N, Samoluk G D and Trefilov A V 1989 *Fiz. Tverd. Tela* **31** 149
[13] Animalu A O E and Heine V 1965 *Phil. Mag.* **12** 1249
[14] Osetsky Yu N, Mikhin A G and Serra A 1993 *J. Nucl. Mater.* at press
[15] Wills J M and Harrison W A 1983 *Phys. Rev.* B **28** 4363
[16] Andersen O K 1975 *Phys. Rev.* B **12** 3060
[17] Dacorogna M 1982 *Phys. Rev.* B **26** 1527
[18] Mikhin A G, Osetsky Yu N and Kapinos V G 1993 *Phil. Mag.* at press
[19] Dickey M and Paskin A 1969 *Phys. Rev.* **188** 1407
[20] Ferrario M and Ryckaert J P 1985 *Mol. Phys.* **53** 587
[21] Brockhouse B N, Abou Helal H E and Hallman E D 1967 *Solid State Commun.* **5** 211
[22] Ye Y-Y, Chen Y, Ho K M, Harmon B N and Lindgard P-A 1987 *Phys. Rev. Lett.* **58** 1769
[23] Smirnov E A 1992 private communication
[24] Kapinos V G, Osetsky Yu N and Platonov P A 1991 *J. Nucl. Mater.* **184** 211
[25] Schaefer H E, Maier K, Weller M, Herlach D, Seger A and Diehl J 1977 *Scripta Metall.* **11** 803
[26] De Schepper L, Cornelis J, Knuyt G, Nihoul J and Stals L 1980 *Phys. Status Solidi* a **61** 341
[27] De Schepper L, Knuyt G and Stals L 1981 *Phys. Status Solidi* a **67** 153
[28] Schultz H 1991 *Landolt–Börnstein New Series* Group III, vol 25, ed H Ullmaier (Berlin: Springer)
[29] Schober H R, Petry W and Trampenau J 1992 *J. Phys.: Condens. Matter* **4** 9321
[30] Hettich G, Mehrer H and Maier K 1977 *Scr. Metall.* **11** 795
[31] Luddehusen M and Maier K 1990 *Acta Metall.* **38** 283
[32] Tsai D H, Bullough R and Perrin R C 1970 *J. Phys. C: Solid State Phys.* **3** 2022